Surface Science 611 (2013) 80–85

Contents lists available at SciVerse ScienceDirect

Surface Science

journal homepage: www.elsevier.com/locate/susc

Mechanical properties of a silicon nanofilm covered with defective graphene

Yuhang Jing [a,b,*], Licheng Guo [a], Yi Sun [a], Jun Shen [b], N.R. Aluru [c]

[a] Department of Astronautical Science and Mechanics, Harbin Institute of Technology Harbin 150001, China
[b] School of Materials Science and Engineering, Harbin Institute of Technology Harbin 150001, China
[c] Department of Mechanical Science and Engineering, Beckman Institute for Advanced Science and Technology, University of Illinois at Urbana-Champaign, Urbana, IL 61801, USA

ARTICLE INFO

Article history:
Received 21 November 2012
Accepted 31 January 2013
Available online 8 February 2013

Keywords:
Si nanofilm
Graphene
Mechanical properties
Defects
Molecular dynamics

ABSTRACT

Molecular dynamics simulations are used to investigate the mechanical properties of a silicon nanofilm covered with a defective graphene. Our results show that graphene not only enhances the mechanical properties of a silicon nanofilm but also unifies the mechanical properties of the ultrathin silicon nanofilms among different crystal orientations. The Young's modulus and critical stress of the silicon nanofilm along four crystal orientations covered with graphene decrease as the thickness of the silicon nanofilm increases. In addition, we study the effects of monoatomic vacancies and Stone–Wales (SW) defects with various concentrations on the mechanical properties of a silicon nanofilm covered with defective graphene. The results show that Young's modulus reduces linearly for monoatomic vacancies and a relatively smaller dependence is observed on SW defects, while the critical stress is more sensitive to the presence of both types of defects. The results in this paper demonstrate the significance of graphene in enhancing the mechanical properties of the silicon nanofilm.

© 2013 Elsevier B.V. All rights reserved.

1. Introduction

Graphene, a two-dimensional (2D) atomic layer of graphite, is attracting great interest due to its outstanding mechanical, thermal, and electronic properties [1]. Graphene has been shown to possess exceptional mechanical properties [2] and it is currently being investigated as a potential reinforcement material for next generation composite materials [3]. Our previous study [4] has shown that graphene can enhance the Young's modulus and critical stress of a silicon film which is one of the most commonly used materials in micro/nanoelectromechanical systems (MEMS/NEMS). Experimental and theoretical investigations have consistently predicted that graphene in its pristine form is the strongest material. The strong inplane sp^2 bonds in graphene and the structural perfection of the honeycomb crystal lattice give rise to an extremely high Young's modulus. Recent experiments have shown that atomic scale defects such as vacancies and dislocations are commonly present in graphene due to experimental techniques such as irradiation with energetic particles [5–8]. The presence of defects would significantly influence the mechanical properties of graphene [9–11]. Molecular dynamic (MD) simulations performed by Neek-Amal reveal that vacancy defects can reduce the Young's modulus and ultimate strength of graphene [12]. Since 2007, graphene-based mechanical devices, such as graphene resonators, have been investigated by Bunch et al. [13]. In addition, ultrathin (12–170 nm) single-crystalline–silicon resonant cantilevers show monotonous degradation in Young's modulus with decreasing thickness [14]. Since the integration of graphene with silicon and silicon-based materials provides an opportunity for the design of MEMS/NEMS devices, it is crucial to understand the mechanical properties of a silicon nanofilm covered with defective graphene. On the one hand it is important to enable design of high-performance and reliable NEMS [15], such as a nanoscale silicon/graphene composite resonant cantilever. On the other hand it can help us see how the ultrathin silicon films affect graphene-based mechanical devices. However, the mechanical properties of a silicon nanofilm covered with defective graphene have not been reported so far.

In this paper, we investigate the mechanical properties of a silicon nanofilm covered with defective graphene using MD simulations. The silicon nanofilms with [100], [110], [111], and [112] crystal orientations are studied. We investigate how the mechanical properties of a silicon nanofilm covered with defective graphene depend on the thickness of the silicon nanofilm. Furthermore, we evaluate the effects of monoatomic vacancies and Stone–Wales (SW) defects with various concentrations on the mechanical properties of a silicon nanofilm covered with defective graphene.

2. Simulation details

In order to study the mechanical properties of a silicon nanofilm covered with graphene, MD simulations are performed using LAMMPS [16]. In our previous study [4], we have shown that the calculated Young's moduli of bulk silicon with the MEAM (1992) [17] or Erhart–Albe [18] potentials are in good agreement with experimental

* Corresponding author at: Department of Astronautical Science and Mechanics, Harbin Institute of Technology Harbin 150001, China. Tel.: +86 451 86418100; fax: +86 451 86403725.
E-mail address: jingyuhang@gmail.com (Y. Jing).

0039-6028/$ – see front matter © 2013 Elsevier B.V. All rights reserved.
http://dx.doi.org/10.1016/j.susc.2013.01.019

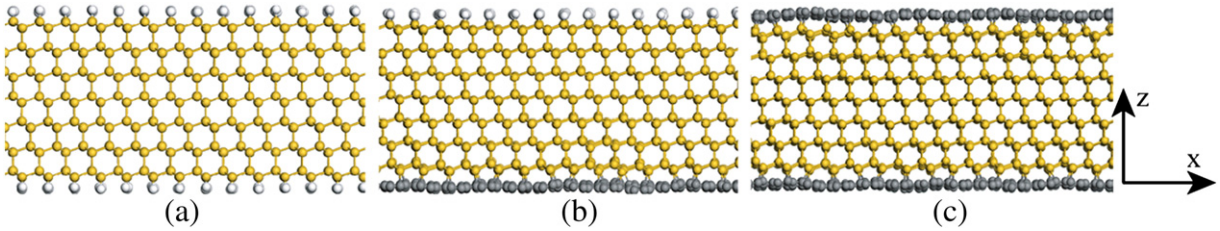

Fig. 1. (Color online) Simulation structures for (a) silicon nanofilm, (b) silicon nanofilm covered with one graphene, and (c) silicon nanofilm covered with two graphenes.

results and DFT calculations. AIREBO [19] potential has also been shown to accurately capture the Young's modulus and fracture strength of bulk graphene as well as bond breaking and bond reforming between carbon atoms [20]. In addition, Erhart–Albe potential is used for Si–C interactions to obtain reasonably relaxed structure for the silicon nanofilm covered with graphene [4]. In this work, we use MEAM (1992) or Erhart–Albe potentials for Si–Si interactions, AIREBO potential for C–C interactions, and Erhart–Albe potential for Si–C interactions. The Si–H interactions are described by Tersoff potential [21], which has been widely used for the SiH system [22,23]. Isothermal–Isobaric (NPT) simulations are performed at a given temperature for 100 ps with a time step of 0.1 fs to let the system reach its equilibrium configuration. The strain is then applied along the uniaxial direction to perform uniaxial tensile tests. The applied strain rate is 0.001/ps. The pressure component vertical to the loading direction is controlled to maintain the uniaxial tensile condition. The strain increment is applied to the structure after every 10,000 time steps with the step size of 0.1 fs. All the MD simulations are carried out at 300 K and the temperature is controlled by employing the Nosé–Hoover thermostat [24]. The Velocity-Verlet algorithm is employed to integrate the equations of motion.

3. Results and discussion

Fig. 1 shows the simulation systems for the silicon nanofilm, silicon nanofilm covered with graphene on one side, and silicon nanofilm covered with graphenes on both sides. Only the silicon nanofilms with [110] crystal orientation are shown in Fig. 1 for brevity. Periodic boundary conditions are imposed on the system along the x- and y-directions. The bottom and top surfaces of the silicon nanofilm and the top surface of the silicon nanofilm covered with one graphene are terminated with H atoms. The thickness of the simulation structure is defined as the mean distance between the bottom and top surfaces. The thickness of the silicon nanofilm is varied from 0.8 to 31.5 nm. To commensurate the graphene with the silicon nanofilms with [100], [110], [111], and [112] crystal orientations, the sizes of the silicon nanofilms with [100], [110], [111], and [112] crystal orientations are chosen as 10.86×10.86, 10.75×10.64, 11.29×11.97, and 9.98×10.64 nm×nm along the x- and y-directions, respectively. The corresponding four graphene structures are modeled with the sizes of 10.82×11.07, 10.82×11.07, 11.32×11.93, and 10.22×10.82 nm×nm along the x- and y-directions, respectively, and most of the mismatches are less than 2% to avoid to induce more stress in graphene or silicon nanofilm. The silicon atoms on the silicon nanofilm surface are initially bonded to the carbon atoms in the graphene. The combined system is fully relaxed until the minimum energy is reached in NPT ensemble. In the fully relaxed, the Si – C bond lengths (0.2–0.22 nm) are close to the crystalline Si – C bond length (0.19 nm), indicating that the bonding strength of Si – C surface bonds is similar to that of crystalline Si – C bonds. During the simulations, the loading direction is always along zigzag direction in graphene in order to compare the results of models with different silicon crystal orientations.

The effects of the thickness of the silicon nanofilm on the mechanical properties of the silicon, Si/Gr (silicon nanofilm covered with graphene on the bottom surface), and Gr/Si/Gr (silicon nanofilm covered with graphene on the top and bottom surfaces) nanofilms are investigated, as shown in Fig. 2. Silicon nanofilms with [100], [110], [111], and [112] crystal orientations are considered. The Erhart–Albe potential is used to describe the Si and Si interactions. As shown in Fig. 2(a), the Young's modulus of the silicon nanofilms increases as the thickness of the silicon nanofilm increases and this trend matches with the previous theoretical results [25]. However, Fig. 2(b) and (c) show that the Young's modulus of Si/Gr and Gr/Si/Gr films increases as the thickness of the silicon nanofilm (for all the four crystal orientations) decreases. These results indicate that the mechanical property of the Si/Gr film depends strongly on the thickness of the silicon nanofilm, which is similar to our previous results for the silicon nanofilm with Si(100)-2×1 surface [4]. Specifically, when the thickness of the silicon nanofilm is about 31.5 nm, the Young's modulus of Si/Gr is higher than that of the silicon nanofilm

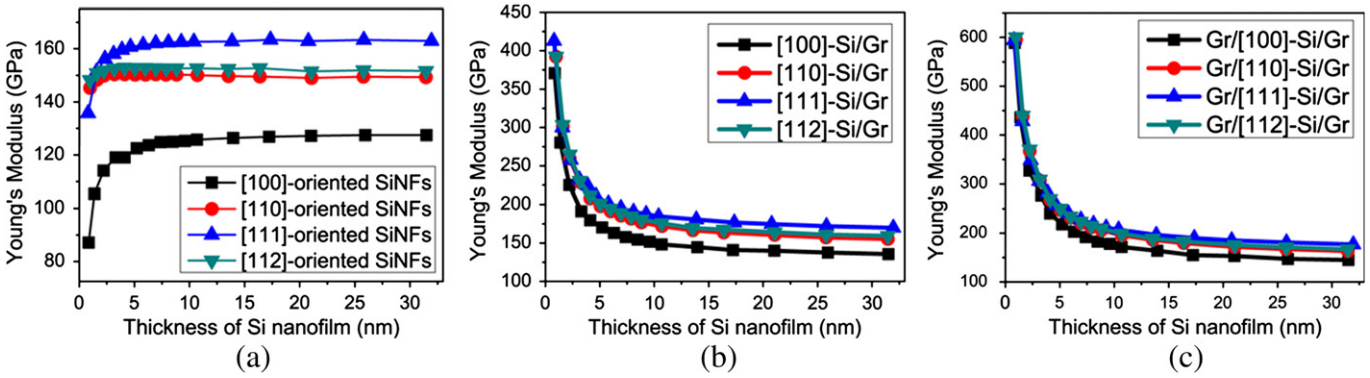

Fig. 2. (Color online) The variation of Young's modulus with the thickness of the Si nanofilm for (a) silicon, (b) Si/Gr, and (c) Gr/Si/Gr structures.

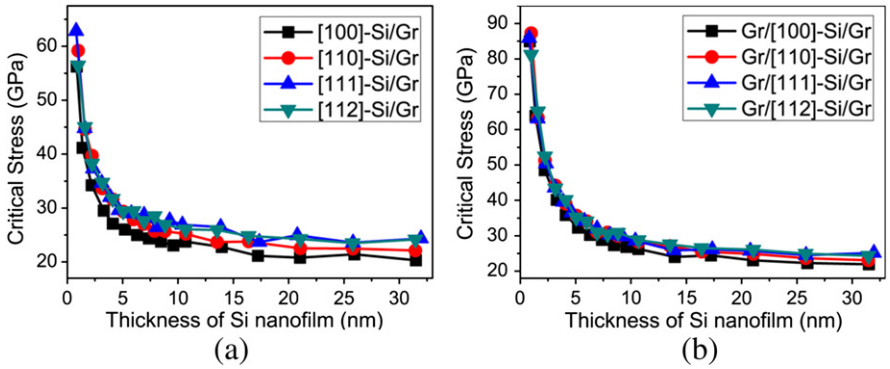

Fig. 3. (Color online) The variation of critical stress with the thickness of the Si nanofilm for (a) Si/Gr and (b) Gr/Si/Gr structures.

by about 6.3%, 4%, 4.2%, and 5% for the silicon nanofilms with [100], [110], [111], and [112] crystal orientations, respectively. The Young's modulus of Gr/Si/Gr is higher than that of the silicon nanofilm by about 13.7%, 9.5%, 8.5%, and 10.1% for the silicon nanofilms with [100], [110], [111], and [112] crystal orientations respectively. However, when the thickness of the silicon nanofilm is about 0.8 nm, the Young's modulus of Si/Gr is higher than that of the silicon nanofilm by about 325.3%, 170.1%, 204.2%, and 164.7% for the silicon nanofilms with [100], [110], [111], and [112] crystal orientations, respectively. The Young's modulus of Gr/Si/Gr is higher than that of the silicon nanofilm by about 575.4%, 309.9%, 337.8%, and 305.2% for the silicon nanofilms with [100], [110], [111], and [112] crystal orientations respectively. Thus, graphene can be a very promising reinforcement nanomaterial for higher modulus untrathin silicon resonant cantilever. However, in comparison, the Young's modulus of graphene is reduced by a larger magnitude due to the presence of silicon films. The calculated Young's modulus and critical stress of graphene along zigzag direction with AIREBO potential is 0.95 TPa and 130.6 GPa, which are consistent with the experimental results [2]. When the thickness of the silicon nanofilm is about 0.8 nm, the highest Young's modulus of Si/Gr among four silicon crystal orientations is lower than that of the graphene by about 56.5%. The highest Young's modulus of Gr/Si/Gr among four silicon crystal orientations is lower than that of the graphene by about 36.8%. The Young's modulus of Si/Gr or Gr/Si/Gr structures is reduced dramatically as the thickness of silicon nanofilm increases. When the thickness of silicon is larger than about 10 nm, the Young's modulus of Si/Gr or Gr/Si/Gr structures decreases slightly. When the thickness of the silicon nanofilm is about 31.5 nm, the highest Young's modulus of Si/Gr among four silicon crystal orientations is lower than that of the graphene by about 82.1%. The highest Young's modulus of Gr/Si/Gr among four silicon crystal orientations is lower than that of the graphene by about 81.4%. Moreover, the Young's modulus of [100]-orientated silicon nanofilm is about 25% lower than that of [111]-orientated silicon nanofilm, independent on the thickness of the silicon nanofilm. The Young's modulus of [100]-Si/Gr nanofilm is about 16% lower than that of [111]-Si/Gr nanofilm. For Gr/Si/Gr nanofilms, the Young's modulus is almost the same for [110], [111], and [112] crystal orientations, and the Young's modulus of Gr/[100]-Si/Gr is a little lower than those of the other three Gr/Si/Gr nanofilms. The results for the critical stress are similar to that of the Young's modulus as shown in Fig. 3.

In order to verify the above simulation results, a different interatomic potential-MEAM potential is adopted to describe the Si–Si interactions and repeat a few calculations. The comparison of Young's modulus and critical stress between MEAM and Erhart–Albe potentials is shown in Fig. 4. The results from Erhart–Albe and MEAM potentials are in reasonable agreement with each other. The above results indicate that graphene can enhance the mechanical properties of the silicon

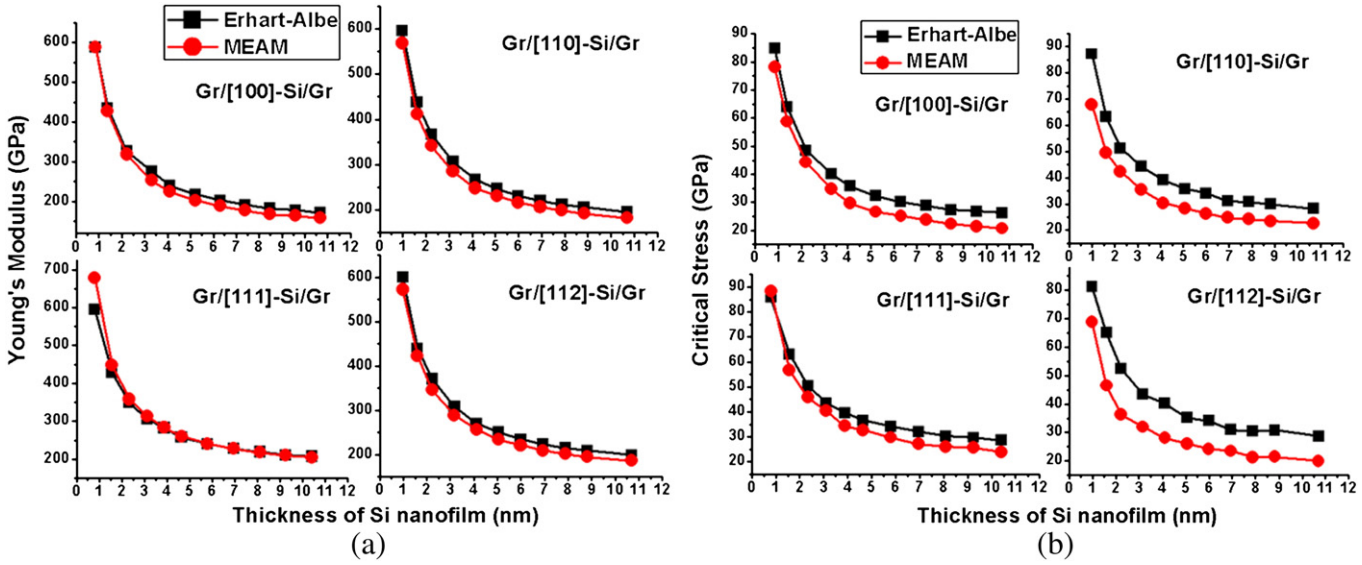

Fig. 4. (Color online) Comparisons of (a) Young's modulus and (b) critical stress for Gr/Si/Gr structure between MEAM and Erhart–Albe potentials.

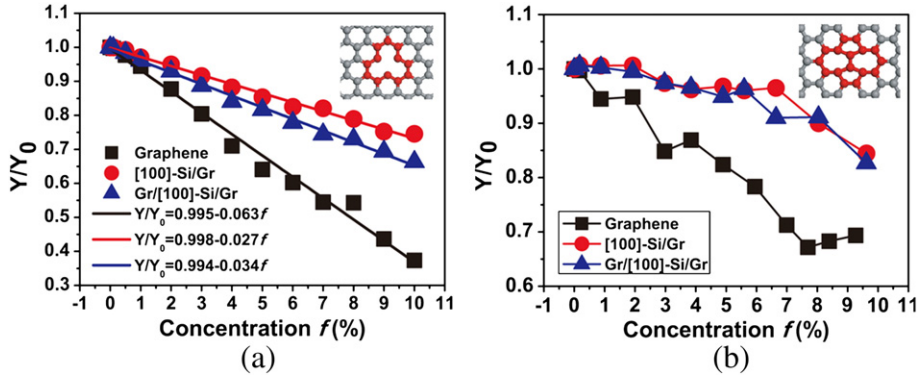

Fig. 5. (Color online) Young's modulus of graphene, Si/Gr, and Gr/Si/Gr structures with (a) monoatomic vacancies and (b) SW defects. Insets in (a): a monoatomic vacancy and (b): a SW defect.

nanofilm along different crystal orientations. In addition, according to construct the Gr/Si/Gr films, graphene can unify the mechanical properties of the silicon nanofilms among different crystal orientations when the thickness of silicon nanofilm is very much thinner. Since the thickness of silicon nanofilm is much thinner, the mechanical properties of Gr/Si/Gr films will be more dependent on the C – C bonds in graphene and C – Si bonds between the graphene and silicon films. When the silicon nanofilm is thinnest, there are only few Si – Si bonds in Gr/Si/Gr films. Furthermore, the Si – Si bond is weaker than the C – C bond and C – Si bond. Thus, the mechanical properties of the silicon nanofilms among different crystal orientations are almost same.

Next, we investigate the effect of monoatomic vacancies and SW defects in graphene on the mechanical properties of graphene, Si/Gr, and Gr/Si/Gr films. We distribute the vacancies and SW defects in the system, by randomly removing atoms and rotating the bonds in a perfect graphene sheet. The concentration f for monoatomic vacancies is defined as the number density of atoms removed from the perfect graphene sheet. For a SW dislocation, f is defined by considering two defective atoms. The thickness of the silicon nanofilm is about 2.2 nm. The Erhart–Albe potential is used to describe the Si and Si interactions. As shown in Fig. 5(a), the Young's modulus Y of defective graphene, [100]-Si/Gr, and Gr/[100]-Si/Gr depend linearly on the monoatomic vacancy concentration. The trend in the variation of Young's modulus with concentration of monoatomic vacancies is consistent with a previous study [12]. Young's modulus Y_0 of a defect-free graphene, [100]-oriented Si/Gr, and Gr/[100]-Si/Gr are 0.95, 0.225, and 0.327 TPa, respectively. Linear fits to Young's modulus in the case of monovacancies are given as $Y/Y_0 = 0.995–0.063f$, $Y/Y_0 = 0.998–0.027f$ and $Y/Y_0 = 0.994–0.034\ f$ for the graphene, Si/Gr, and Gr/Si/Gr films, respectively. For SW defects, as shown in Fig. 5(b), a relatively slower decrease in Young's modulus is observed for defective graphene, [100]-Si/Gr, and Gr/[100]-Si/Gr. This can be explained by noting that SW defects maintain interatomic sp^2 bonding while monoatomic vacancies break the perfection of pristine sheet. We note

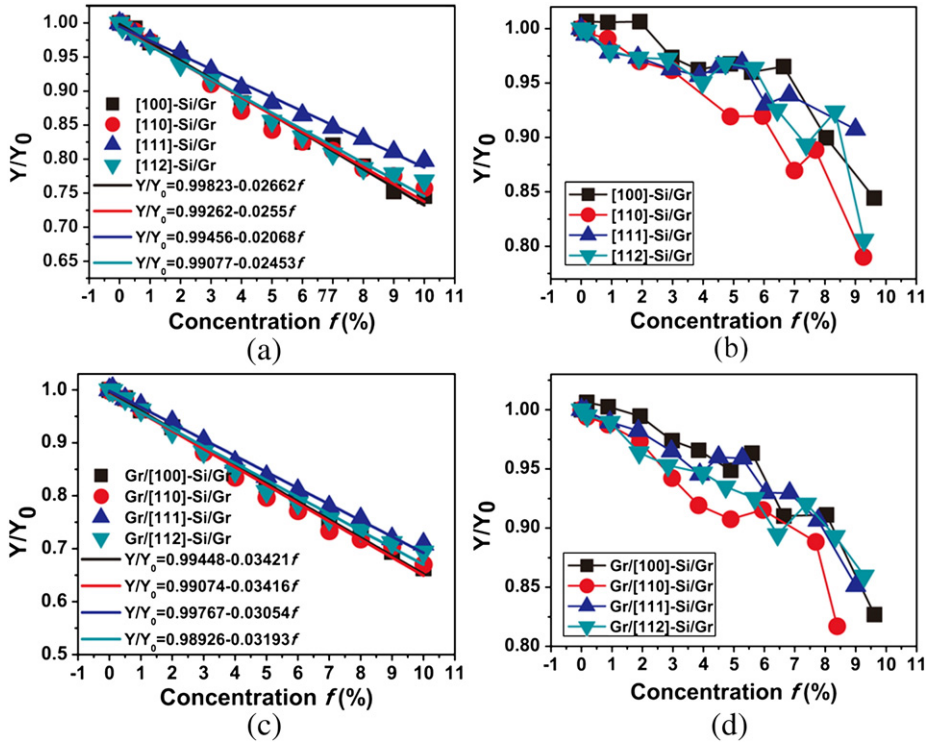

Fig. 6. (Color online) Young's modulus of Si/Gr and Gr/Si/Gr structures along four crystallographic directions with (a), (c) monoatomic vacancies and (b), (d) SW defects.

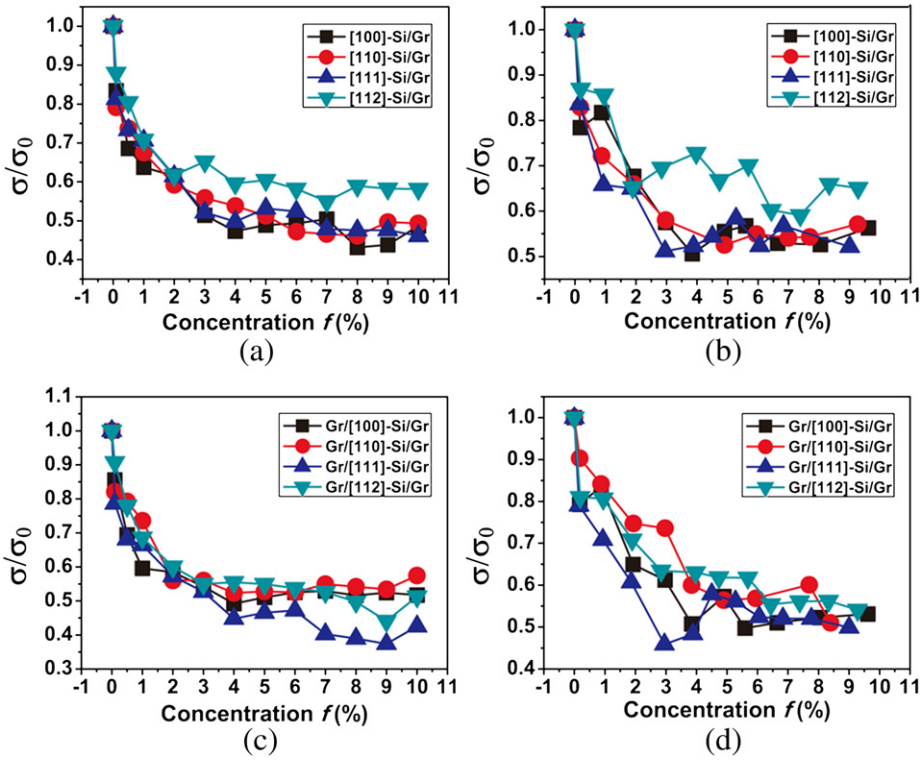

Fig. 7. (Color online) Critical stress of Si/Gr and Gr/Si/Gr structures along four crystallographic directions with (a), (c) monoatomic vacancies and (b), (d) SW defects.

that monoatomic vacancies and SW defects have larger impact on the Young's modulus of graphene than on Si/Gr and Gr/Si/Gr films. When the vacancy concentration is 10%, the Young's modulus of Si/Gr and Gr/Si/Gr nanofilms are 167.8 and 216.9 GPa, which are larger than that of the silicon nanofilm (114.2 GPa). Therefore, defective graphene can also enhance the mechanical properties of the silicon nanofilm. Fig. 6 shows the Young's modulus of Si/Gr and Gr/Si/Gr nanofilms along four crystallographic directions with monoatomic vacancies and SW defects. It can be observed that Young's modulus of Si/Gr or Gr/Si/Gr film reduces linearly with concentration of monoatomic vacancies as shown in Fig. 6(a) and (c). A relatively weaker dependence of Young's modulus on SW defects is observed as shown in Fig. 6(b) and (d).

In contrast to the gentle dependence of Young's modulus, the critical stress is more sensitive to the presence of these two defects. Fig. 7 shows the variation of critical stress with monoatomic vacancies and SW defects for Si/Gr and Gr/Si/Gr films along four crystallographic directions. We note that the critical stress is reduced to half its value by introducing monoatomic vacancies or SW defects at a concentration of 3%. We also find that if $f > 3\%$, the amount of critical stress reduction will be maintained at approximately 50%, because the determining factor for critical stress is the weakest cross-section. The failure patterns in the Gr/Si/Gr nanofilm with 0.1 and 5% monoatomic vacancies are shown in Fig. 8. It can be observed that the failure of Gr/Si/Gr nanofilm with 5% monoatomic vacancies (Fig. 8b) is extremely localized with no diagonal crack propagation.

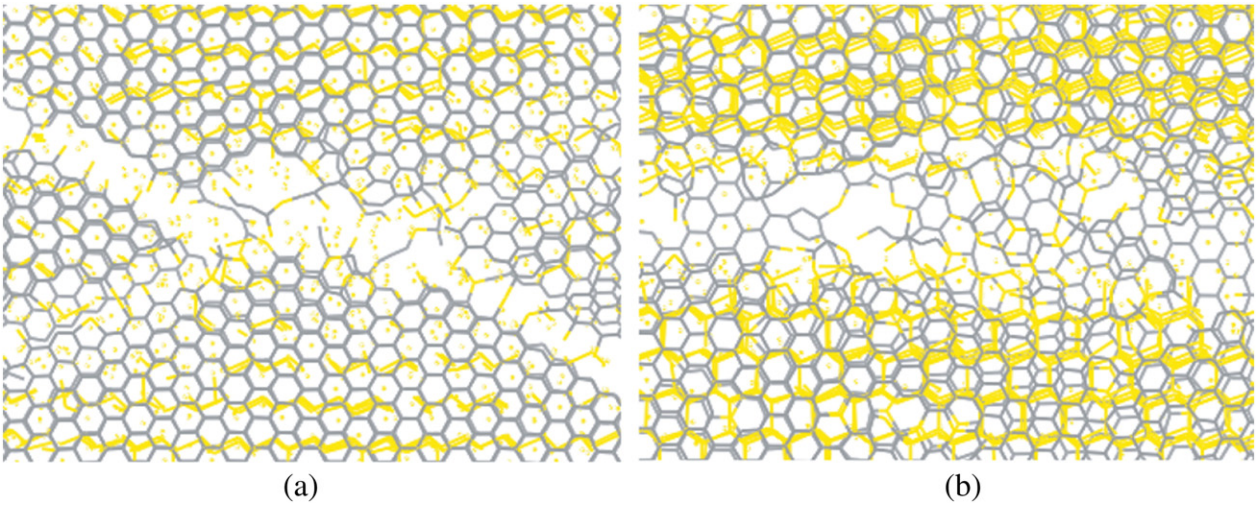

Fig. 8. (Color online) Failure patterns in Gr/Si/Gr nanofilm with (a) 0.1 and (b) 5% monoatomic vacancies.

However, a diagonal crack propagation is observed in the Gr/Si/Gr nanofilm with 0.1% monoatomic vacancies (see Fig. 8a).

4. Conclusions

In this paper, we investigated the mechanical properties of a silicon nanofilm covered with perfect and defective graphene using MD simulations. A very large magnitude enhancement (up to 575.4%) in the Young's modulus of Gr/Si/Gr films relative to ultrathin silicon nanofilm was found. The Young's modulus and critical stress of the silicon nanofilm along four crystal orientations covered with graphene decrease as the thickness of the silicon nanofilm increases. Therefore, graphene can be a very promising reinforcement nanomaterial for higher modulus ultrathin silicon resonant cantilever. In addition, according to construct the Gr/Si/Gr films, graphene can unify the mechanical properties of the silicon nanofilms among different crystal orientations when the thickness of silicon nanofilm is very much thinner where the stronger C – C bonds in graphene and C – Si bonds between the graphene and silicon films may dominate the mechanical properties of Gr/Si/Gr films. Furthermore, we study the effect of monoatomic vacancies and SW defects with various concentrations on the mechanical properties of a silicon nanofilm covered with defective graphene. It is found that Young's modulus reduces linearly for monoatomic vacancies and a relatively smaller dependence is observed on SW defects. We explain that the SW defects maintain interatomic sp^2 bonding while monoatomic vacancies break the perfection of pristine sheet. The critical stress is more sensitive to the presence of monoatomic vacancies and SW defects and a significant reduction in critical stress is observed.

Acknowledgment

This research was supported by the National Science Foundation under grant nos. 0941497 and 1127480, Fundamental Research Funds for the Central Universities under grant no. HIT.NSRIF.2013031 and China Postdoctoral Science Foundation.

References

[1] A.K. Geim, K.S. Novoselov, Nat. Mater. 6 (2007) 183.
[2] C. Lee, X. Wei, J.W. Kysar, J. Hone, Science 321 (2008) 385.
[3] X. Zhao, Q. Zhang, D. Chen, P. Lu, Macromolecules 43 (2010) 2357.
[4] Y. Jing, N.R. Aluru, Comput. Mater. Sci. 50 (2011) 3063.
[5] D. Sen, K. Novoselov, P.M. Reis, M.J. Buehler, Small 6 (2010) 1108.
[6] S.S. Verbridge, R. llic, H.G. Craighead, J.M. Parpia, Appl. Phys. Lett. 93 (2008) 013101.
[7] J. Kotakoski, A.V. Krasheninnikov, U. Kaiser, J.C. Meyer, Phys. Rev. Lett. 106 (2011) 105505.
[8] A. Hashimoto, K. Suenaga, A. Gloter, K. Urita, S. Iijima, Nature 430 (2004) 870.
[9] M. Neek-Amal, F.M. Peeter, Appl. Phys. Lett. 97 (2010) 153118.
[10] J.R. Xiao, J. Staniszewski, J.W. Gillespie, Compos. Struct. 88 (2009) 602.
[11] Q. Lu, B. Bhattacharya, Nanotechnology 16 (2005) 555.
[12] M. Neek-Amal, F.M. Peeter, Phys. Rev. B 81 (2010) 235437.
[13] J. Scott Bunch, A.M. van der Zande, S.S. Verbridge, et al., Science 315 (2007) 490.
[14] X. Li, T. Ono, Y. Wang, M. Esashi, Appl. Phys. Lett. 83 (2003) 3081.
[15] X. Li, B. Bhushan, K. Takashima, C. Baek, Y. Kim, Ultramicroscopy 97 (2003) 481.
[16] S. Plimpton, J. Comput. Phys. 117 (1995) 1.
[17] M.I. Baskes, Phys. Rev. B 46 (1992) 2727.
[18] P. Erhart, K. Albe, Phys. Rev. B 71 (2005) 035211.
[19] S.J. Stuart, A.B. Tutein, J.A. Harrison, J. Chem. Phys. 112 (2000) 6472.
[20] H. Zhao, K. Min, N.R. Aluru, Nano Lett. 9 (2009) 3012.
[21] F. de Brito Mota, J.F. Justo, A. Fazzio, J. Appl. Phys. 86 (1999) 1843.
[22] K. Jarolimek, R.A. de Groot, G.A. de Wijs, M. Zeman, Phys. Rev. B 82 (2010) 205201.
[23] J. Houska, J.E. Klemberg-Sapieha, L. Martinu, J. Appl. Phys. 107 (2010) 083501.
[24] W.G. Hoover, Phys. Rev. A 31 (1985) 1695.
[25] A.I. Fedorchenko, A. Wang, H.H. Cheng, Appl. Phys. Lett. 94 (2009) 152111.